Separation of Light Liquid Paraffin C₅–C₉ with Cuban Volcanic Glass Previously Used in Copper Elimination from Water Solutions

Miguel Autie-Pérez [1,*], **Antonia Infantes-Molina** [2], **Juan Antonio Cecilia** [2] (ID),
Juan M. Labadie-Suárez [1] **and Enrique Rodríguez-Castellón** [1,*] (ID)

[1] Departamento FQB, Facultad de Ingeniería Química, Instituto Superior Politécnico José Antonio Hechevarría, MES, La Habana 19390, Cuba; Labadie.Bol2014@gmail.com

[2] Departamento de Química Inorgánica, Cristalografía y Mineralogía (Unidad Asociada al ICP-CSIC), Facultad de Ciencias, Universidad de Málaga, Málaga 29071, Spain; ainfantes@uma.es (A.I.-M.); jacecilia@uma.es (J.A.C.)

[*] Correspondence: aautie@gmail.com (M.A.-P.); castellonl@uma.es (E.R.-C.); Tel.: +53-7-267-6104 (M.A.-P.); +34-952-131-873 (E.R.-C.)

Featured Application: In this work, an inexpensive and available material, as volcanic glass, is used to absorb metals from wastewater and then it is used to the separation of light liquid-olefins.

Abstract: Raw porous volcanic glass from Cuba was used as an adsorbent for Cu^{2+} removal from dyes after activation with an acid solution. After Cu^{2+} adsorption, it was also evaluated its capacity to separate n-paraffins from a mixture by inverse gas chromatography (IGC), and the results were compared with those obtained with bare volcanic glass without copper. The main goal of this work is to highlight the great applicability of natural volcanic glass, which can be reused without pretreatment as an adsorbent. The results from copper adsorption were quite promising, considering the availability and low cost of this material; the sample without acid treatment turned out to be the most adequate to remove copper. Moreover, the results from IGC revealed that the separation of paraffins from the mixture was achieved with both bare volcanic glass and glass containing Cu, although greater heat adsorption values were obtained when copper was present in the sample due to the stronger interaction between paraffin and copper. The high availability and low cost of this porous material make it a potential and attractive candidate to be used in both heavy metal removal and paraffin separation for industrial purposes.

Keywords: glass; adsorption; surface properties; copper removal; IGC; paraffins

1. Introduction

Despite the decline in oil reserves, dependence on the petrochemical industry is still high, since there is no alternative energy source able to satisfy the demands of the world's population. Treatment of crude gives rise to a range of valuable products, such as fuels, waxes, asphalt, polymers, plastics, paints, tires, and detergents. Among the most important oil fractions are the short paraffins (C_nH_{2n+2}), since these compounds are main components of fuel and natural gas that have relatively low toxicity, because their combustion only generates CO_2.

A challenge for the petrochemical industry is olefin/paraffin separation, since both display similar physicochemical properties [1]. The use of membranes, cryogenic distillation, and absorption have emerged as potential methods for the separation of paraffin/olefin [2–5]. Among them, the most

sustainable technology is related to selective adsorption of olefins, since its insaturation favors stronger interactions with the adsorbent [4]. However, the interaction of paraffins is more limited, since these compounds are only formed of C–C and C–H bonds, so the adsorption should take place through nonspecific interactions.

Traditionally, molecular sieves such as zeolites [6,7], activated carbons [8,9], and metal-organic frameworks (MOFs) [10,11], which display cavities with a specific pore size, have been used as efficient sieves to separate paraffin. However, these compounds also have some drawbacks related to the low thermal stability of the MOFs and the cost of synthesizing molecular sieves with appropriate pore size at a large scale. Currently, companies demand competitive adsorbents with lower production costs in order to increase the profit margin.

Natural clay minerals and zeolites are abundant and inexpensive natural molecular sieves that have been used in several adsorption processes [12–14] and paraffin separation [7]. Similarly, volcanic glass, a less well-known material than zeolites or clay minerals, has shown interesting behavior in the adsorption of harmful cations [15,16] and dyes [17–19] and in the separation of olefin/paraffin [20]. So volcanic glass should be considered as a potential adsorbent to separate *n*-paraffins. The genesis of volcanic glass takes place by a sudden cooling of the magma, obtaining a quasi-stable and amorphous structure [21]. The most abundant volcanic glass is obsidian, which was used as a knife blade or scalpel blade since prehistory [22,23]. Volcanic glass is a material that displays low thermal conductivity, low density, and high resistance to fire and perlite aggregate plasters. Hydration of obsidian leads to perlite, which shows a wider range of applications due to its high adsorption of sound, low bulk density, low thermal conductivity, and fire resistance, all of which provides interesting properties when used in the construction industry as plaster, insulation boards, and concrete, as well as a soil conditioner or carrier for herbicides, insecticides, and chemical fertilizers. In addition, perlite can be used for filtering water and other liquids, in food processing, and in pharmaceutical manufacturing [24]. Volcanic glass has also been used as starting material in the synthesis of clay minerals [25], as smectites, or as zeolites [26,27].

The aim of this research is to evaluate Cuban volcanic glass in two consecutives processes, the adsorption of transition metal cations and then its application to the separation of liquid paraffins. The adsorption capacity of volcanic glass was evaluated using Cu^{2+} cations as target metal. Cu species are considered pollutants from the mineral and metallurgic industries. The wastewater is a very dangerous environmental problem: it has nonbiodegradability features; it is hazardous to animal and human health, since the pollutants accumulate in living tissue, causing many harmful effects; it is implicated in biochemical and biological oxidation processes; and it causes serious problems in wastewater treatment plant sludge [28]. Several methods, such as precipitation, ion exchange, solvent extraction, and adsorption on oxides, have been shown to be highly efficient in heavy metal removal. Copper content should be less than 1.3 parts per million, since that is the limit for human consumption according to the US Environmental Protection Agency [29]. However, the high maintenance cost of these methods does not suit the need, mainly in developing countries [30].

Then, raw volcanic glass and Cu-volcanic glass were evaluated to separate liquid n-paraffins (C_5–C_9) by inverse gas chromatography (IGC) as alternative method to the traditional distillation employed in the petrochemical industry. The use of IGC to separate liquid paraffins has been studied in the literature, and interesting values have been attained for porous hexacyanocobaltates [31], metal-organic framework (Cu-BTC and Fe-BTC) [10], and even inexpensive materials such as natural clinoptilolite [7]. IGC evaluates both the surface and bulk properties of porous materials. This technique is highly efficient in analyzing the physicochemical properties of nonvolatile materials, such as diffusion coefficient, crystallinity, or specific parameters of surface free energy [32,33], which provides interesting information in nanomaterials [34,35], fibers [36], and polymer and coatings [37,38], as well as in the pharmaceutical industry.

2. Materials and Methods

2.1. Volcanic Glass

The studied material was volcanic glass extracted from Ají de la Caldera, Cuba. The volcanic glass, sieved to obtain a fraction lower than 0.1 mm, was activated with H_2SO_4 solution (0.2–0.6 mol L^{-1}) by stirring at 298 K for 4 h. Later, the samples were washed with water until the sulfate species were removed. Then the samples were dried in an oven at 383 K.

2.2. Characterization of the Materials

Elemental bulk composition of the sample was determined by wavelength-dispersive X-ray fluorescence (WDXRF) spectrometry using an ARL ADVANT'XP spectrometer under vacuum. Samples were dried and calcined and prepared as 35 mm diameter fused beads in a Katanax K1 machine. The composition was determined by using UniQuant software.

X-ray diffraction (XRD) patterns of the sample were obtained with an X'Pert PRO MPD diffractometer (PANanalytical) equipped with a Ge (111) primary monochromator using Cu $K_{\alpha 1}$ (1.5406 Å) radiation.

Diffuse Reflectance Infrared Fourier Transform (DRIFT) spectra were collected on a Harrick HVC-DRP cell fitted to a Varian 3100 FTIR spectrophotometer. The interferograms consisted of 120 scans, and the spectra were collected using a KBr spectrum as background. About 30 mg of finely ground sample was placed in a sample holder.

The textural properties (S_{BET}, V_p, d_p) of the volcanic glass were determined by N_2 adsorption-desorption at 77 K in a Micromeritics ASAP 2020 apparatus. Prior to analysis, volcanic glass was outgassed at 273 K and 0.01 kPa for 12 h. The specific surface area was determined using the Brunauer-Emmett-Teller equation considering an N_2 molecule cross-section of 16.2 $Å^2$ [39]. The total pore volume was calculated from the adsorption isotherm at $P/P_0 = 0.99$.

Size and morphology of the nanoparticles were studied by high-resolution transmission electron microscopy using a TALOS F200x instrument. TEM analysis was performed at 200 kV and 5.5 A and scanning transmission electron microscopy with a High Angle Annular Dark Field (HAADF) detector, at 200 kV and 200 nA.

X-ray photoelectron spectra were collected using a Physical Electronics PHI 5700 spectrometer with nonmonochromatic Mg Kα radiation (300 W, 15 kV, and 1253.6 eV) with a multichannel detector. Spectra were recorded in the constant pass energy mode at 29.35 eV, using a 720 μm diameter analysis area. Charge referencing was measured against adventitious carbon (C 1*s* at 284.8 eV). A PHI ACCESS ESCA-V6.0 F software package was used for acquisition and data analysis.

2.3. Cu^{2+} Adsorption Tests

Cu^{2+} adsorption was carried out from a solution of $CuCl_2 \, 2H_2O$ (1 mol L^{-1}) (Merck, analysis grade), using a range of concentrations between $1 \, 10^{-3}$ and $1 \, 10^{-1}$ mol L^{-1}.

The batch adsorption experiments were performed by immersing 100 mg of adsorbent with 10 mL of copper solution and stirring for 4 h. Then the solid was removed by filtration, while the liquid was analyzed in a UV-vis spectrophotometer, model Shimadzu UV mini-1240, at a wavelength of 600 nm. Cu adsorbed per unit mass adsorbent (mol g^{-1}) at equilibrium was calculated using the mass balance described by Equation (1):

$$q = \frac{V \times (c_0 - c_{eq})}{m_{ads}} \tag{1}$$

where V (mL) is the volume of the sample solution, c_0 and c_{eq} (mmol mL^{-1}) are the copper concentrations initially and after adsorption equilibrium is reached, q (mmol g^{-1}) is the amount of Cu adsorbed onto the volcanic glass, and m_{ads} (g) is the sample mass.

The adsorption isotherms were adjusted to the Langmuir model [40], assuming that each site can hold at most one molecule on a homogeneous surface, from Equation (2):

$$q = \frac{q_{max} \times K_L \times c_{eq}}{1 + (K_L \times c_{eq})} \tag{2}$$

where q_{max} (mmol g^{-1}) is the maximum adsorbed concentration, c_{eq} (mmol mL^{-1}) is the concentration of copper in solution at equilibrium, and K_L (L mg^{-1}) is the Langmuir constant.

2.4. Separation of N-Paraffin Tests

The IGC data were recorded with Shimadzu equipment (model 14B) and a flame ionization detector in the 403–488 K temperature range. Helium was used as a carrier gas at a flow rate of 12.8 cm^3/min. Previously cleaned and weighed stainless steel columns (60 cm long, 2.2 mm inner diameter) were packed with 2.5 g of the material. The packed columns were outgassed overnight at 523 K under helium flow. N-Alkanes of analytical grade were used in all cases and injected as the smallest detectable amount of their vapor phase extracted from the head space of their containers, to obtain data close to Henry adsorption coverage.

To obtain the corrected retention times for the probes, the relation $(t_R - t_0)$ was used, where t_0 is the retention time of methane, CH$_4$ (unretained hydrocarbon), and t_R is the retention time of the probe. The corrected retention times were taken as the average value among three injections. Mixtures of C$_1$-(C$_5$-C$_9$) were prepared by introducing a small quantity of CH$_4$ in the head space of each liquid alkane, and C$_5$-C$_9$ net retention volumes, V_n, were calculated according to Equation (3):

$$V_n = J \cdot V_f \cdot (t_R - t_0) \cdot \frac{T_c}{T_A} \cdot \frac{(P_0 - P_w)}{P_0} \tag{3}$$

where J is the James-Martin gas compressibility correction factor, V_f is the gas carrier flow rate at the flow meter temperature T_f, T_C is the column temperature, T_A is the room temperature ($T_A = T_f$), P_0 is the outlet pressure, and P_w is the vapor pressure of water at T_f.

The differential adsorption heat, Q_d, equal to the enthalpy for the standard adsorbed state ΔH_{d0} (within the Henry zone), was determined from the slope of ln (V_n/A_S) versus $1/T_C$ plot according to Equation (4):

$$Q_d = \Delta H_{d0} = -R \cdot \frac{d[\ln(V_n/A_S)]}{d(1/T_c)} \tag{4}$$

where R is the universal gas constant and A_S is the product of the specific surface area (S) and the amount of sample (m) in the column.

3. Results and Discussion

Characterization of Volcanic Glass

The elemental bulk composition of volcanic glass evaluated from X-ray Fluorescence Spectrometer (XRFS) analysis shows how this material is mainly composed and Si and Al, with small proportions of K, Fe, Ni, Ca, and Na. Previous research has pointed out that the viscosity of volcanic glass is directly related to the SiO$_2$ content [21]. Thus, volcanic glass with low SiO$_2$ content (<50%) is less viscous than glass with SiO$_2$ content above 65%. Considering the SiO$_2$ concentration shown in Table 1, the Cuban volcanic glass must display low fluency and high viscosity, probably due to slow cooling [21].

Table 1. Chemical composition of volcanic glass and Cu-volcanic glass (%).

Sample	SiO_2	Al_2O_3	K_2O	Fe_2O_3	CuO	MgO	CaO	Na_2O
Volcanic Glass	66.2	13.4	2.4	2.8	–	1.3	2.5	1.7
Cu-Volcanic Glass	63.3	12.2	3.6	3.4	2.2	1.9	1.8	1.2

The textural parameters of volcanic glass were determined from N_2 adsorption-desorption at 77 K (Figure 1). According to the International Union of Pure and Applied Chemistry (IUPAC) classification, the adsorption isotherm can be adjusted to type II [41], which is typical of nonporous or macroporous materials. Nonetheless, the N_2 adsorbed at lower relative pressure indicates that this volcanic glass also displays slight microporosity. The hysteresis loop can be considered as type H3, which is given by nonrigid aggregates of platelike particles (e.g., certain clays), but also if the pore network consists of macropores that are not completely filled with pore condensate [41]. The specific surface area, estimated by the Brunauer-Emmett-Teller equation [39], determined a low specific surface area (51 m^2/g), with a pore volume of 0.083 cm^3/g. After Cu exchange, the specific surface area was lower (19 m^2/g). Considering the low specific surface area and the macroporosity, the N_2 adsorbed must be attributed to the fillings between adjacent particles.
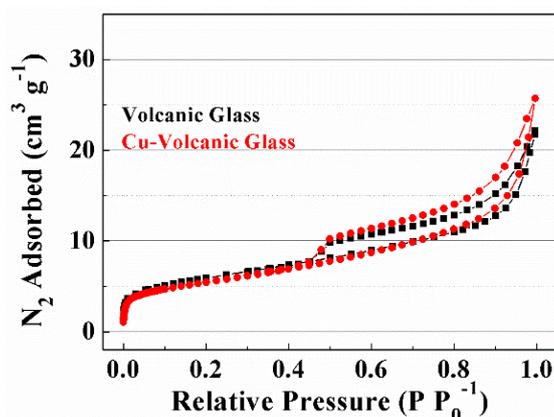
Figure 1. N_2 adsorption-desorption at 77 K of volcanic glass and Cu-volcanic glass.

According to the data of raw volcanic glass reported previously [20], XRD of volcanic glass hardly displays defined diffraction peaks. A broad band can be observed at $2\theta = 20–30°$ which is attributed to the amorphous structure of volcanic glass. In addition, the existence of a pseudo-amorphous phase of aluminosilicate and Ca_3SiO_5 species, which shows higher crystallinity, is noteworthy.

As indicated previously [20], the FTIR spectrum of volcanic glass displays a broad signal between 3000 and 3700 cm^{-1}, which corresponds to –OH groups. Thus, the band located at 3620 cm^{-1} is assigned to structural OH-stretching, and those at 3420 cm^{-1} and 1640 cm^{-1} correspond to OH stretching and bending vibrational bands of adsorbed water [42]. After Cu incorporation, the broad signal remains, but the contribution located at 3620 cm^{-1} decreases in intensity, indicating that Cu interacts with OH groups. On the low wavelength side, Si–O stretching bands are located at 1148 cm^{-1}, 991 cm^{-1}, and 804 cm^{-1} [43,44]. The band at 908 cm^{-1} corresponds to the bending mode of Al–OH [43]. Raw volcanic glass also displays a weak shoulder band centered at ~1425 cm^{-1} and attributed to CO_3^{-2} species, which must interact with the Ca^{2+} and Mg^{2+} species [45], reported in Table 1.

In order to evaluate the chemical composition of the surface of volcanic glass, X-ray Photoelectron Spectroscopy (XPS) analysis was performed for the raw material (Table 2). Similar to the elemental bulk composition (Table 1), Si and Al are the main elements in volcanic glass. In addition, the presence of other elements is noted, such as Mg and Ca, which can partially replace Al^{3+} sites by other Mg^{2+} ones, as well as carbonates and hydroxides, confirmed from the C 1s core level spectrum. The small

amounts of Na^+ and K^+ can be used to counterbalance the charge deficiency of the aluminosilicate. In all cases, the binding energies are attributed to oxide species, except in the case of the O 1s core level spectrum, where two contributions, located at 532.4 and 531.4 eV, are detected (Figure 2) [46]. These contributions are attributed to the coexistence of oxide and hydroxide or carbonate species.

Table 2. Atomic concentration on the surface (%).

Sample	O 1s	Si 2p	Al 2p	Mg 2p	Ca 2p	Na 1s	K 1s	Cu 2p
Volcanic Glass	61.5	19.8	3.7	2.8	1.6	0.7	0.7	–
Cu-Volcanic Glass	62.1	19.9	3.8	2.2	0.9	0.7	0.7	0.6
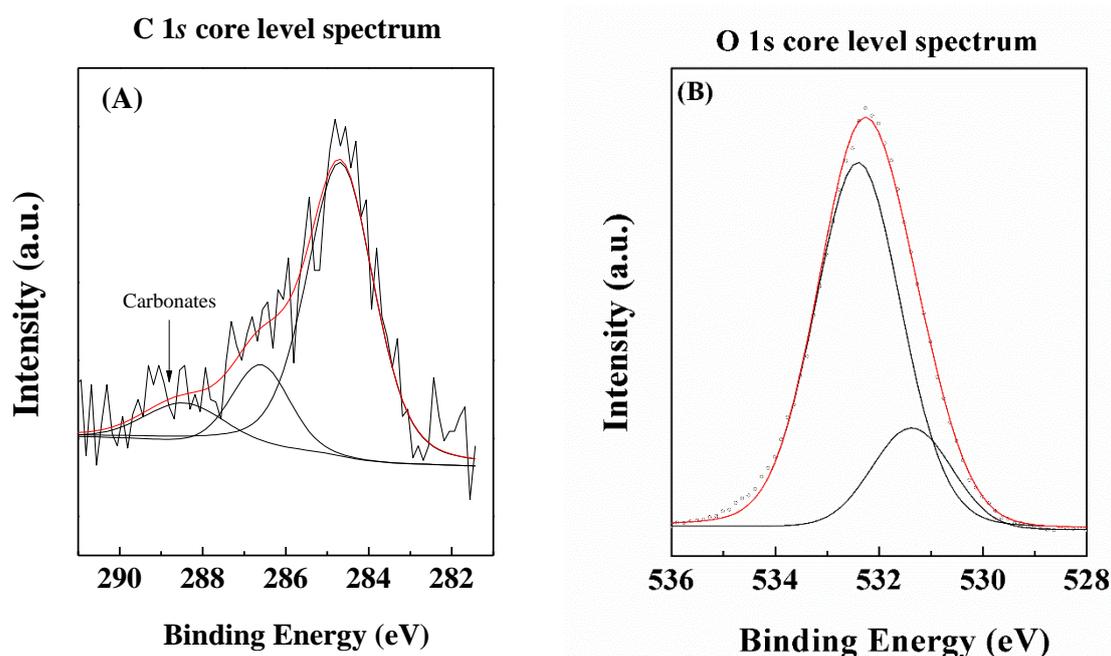
Figure 2. C 1s core level spectrum and O 1s core level spectrum of Cu-volcanic glass.

4. Cu^{2+} Adsorption Capacity of Volcanic Glass

The elemental composition of volcanic glass mainly consists of aluminosilicates, similar to clay minerals and zeolites, although its structure is amorphous. Previous research has established that an increase in temperature should cause an expansion of the amorphous structure; however, this thermal treatment can also produce dehydroxilation of the –OH groups, which are involved in the process of Cu adsorption [46], as indicated by the following reaction:

$$–Si–OH + Cu^{2+} \leftrightarrow Si–O–Cu^+ + H^+ \text{ or } –Al–OH + Cu^{2+} \leftrightarrow Al–O–Cu^+ + H^+$$
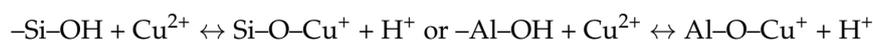
The isotherm adsorption data (Figure 3) show how Cu adsorption decreases when volcanic glass is activated with more concentrated H_2SO_4 solutions, following the trend H_2SO_4 (0.0 M) > H_2SO_4 (0.2 M) > H_2SO_4 (0.4 M) > H_2SO_4 (0.6 M) due to modification of the point of zero charge of the volcanic glass [17,47]. These data are in agreement with the literature, since the heavy metal adsorption takes place in a narrow pH range [47–49]. In the case of adsorption of Cu^{2+} species, it has been reported that Cu adsorption increases at higher pH values [24,47]. Under these activation conditions, the leaching of volcanic glass must be discarded, since it requires stronger conditions [50,51].
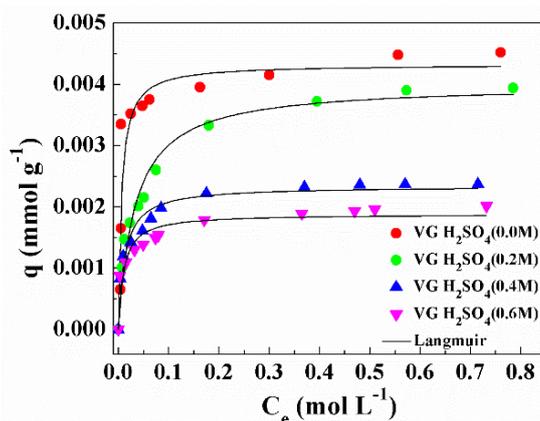
Figure 3. Cu^{2+} adsorption in volcanic glass (VG) with acid treatment and activated with H_2SO_4 (0.2 M, 0.4 M, and 0.6 M) solution.

The isotherm data were fitted to the Langmuir model (Table 3). These data reveal that volcanic glass without previous acid treatment reaches the q_{max} maximum value ($4.32 \cdot 10^{-4}$ mol g^{-1}); however, the q_{max} value decreases accordingly as the H_2SO_4 concentration used in the prior activation increases. The strength of the adsorbate-adsorbent interaction, defined by the K_L value, shows how volcanic glass without acid activation exhibits a stronger interaction.

Table 3. Equilibrium adsorption parameters according to the Langmuir model to Cu^{2+} adsorption on volcanic glass.

Sample	$q_{max} \times 10^3$ (mmol g^{-1})	K_L (L g^{-1})	R
Volcanic Glass (H_2SO_4 0.0 M)	4.32 ± 0.27	2.5 ± 0.9	0.96
Volcanic Glass (H_2SO_4 0.2 M)	4.00 ± 0.14	1.5 ± 0.5	0.97
Volcanic Glass (H_2SO_4 0.4 M)	2.34 ± 0.07	1.2 ± 0.2	0.96
Volcanic Glass (H_2SO_4 0.6 M)	1.81 ± 0.08	0.5 ± 0.1	0.94

Since volcanic glass without previous acid activation reached maximum adsorption capacity, this material was recycled to evaluate its behavior in liquid paraffin separation. Prior to this study, volcanic glass was characterized after the adsorption process to show the Cu adsorbed.

The elemental bulk composition of Cu-volcanic glass was evaluated from XRFS analysis (Table 1). These data indicate that the amount of Cu (in the form of CuO) after the adsorption process was 2.2%, while the amounts of other elements were close to that shown for raw volcanic glass, which discards the leaching of these elements along the adsorption process or along the acid activation. In the same way, the chemical composition on its surface was determined by XPS, reaching a Cu content of 0.6% (Table 2). The Cu 2p core level spectrum displays a main peak at about 932.8 eV, which is ascribed to Cu^{2+} species in the form of CuO, while the other contribution, located at about 935.2 eV, is assigned to the shake-up satellite, which is typical of bivalent cations [52]. From the atomic concentrations, a slight decrease of the Mg and Ca species on its surface can be observed, which could indicate partial leaching of these species or deposition of the Cu species in these zones.

Finally, the Cu content on its surface was also confirmed by TEM (Figure 4). This micrograph shows how Cu^{2+} species are distributed on the surface in some parts of volcanic glass; in other parts, it is not present. Energy-Dispersive X-ray spectroscopy (EDX) analysis confirms that the zones where copper is present correspond with the presence of carbon, and therefore its distribution on the surface depends on carbonate location. These data corroborate that Cu incorporation takes place from the intercalation of Cu with Ca from calcite in the pristine mineral. The data could be in agreement with

the adsorption data, since the incorporation of Cu^{2+} species must take place by a cationic exchange of Mg^{2+} or Ca^{2+} by Cu^{2+} species, which is in agreement with the atomic concentrations on the surface (Table 2). The reaction that takes place with the carbonate species should be:

$$(Ca_xMg_y)CO_3 + 2Cu^{2+} \rightarrow (Ca_{x-1}Mg_{y-1}Cu_2)\,CO_3 + Mg^{2+} + Ca^{2+}$$
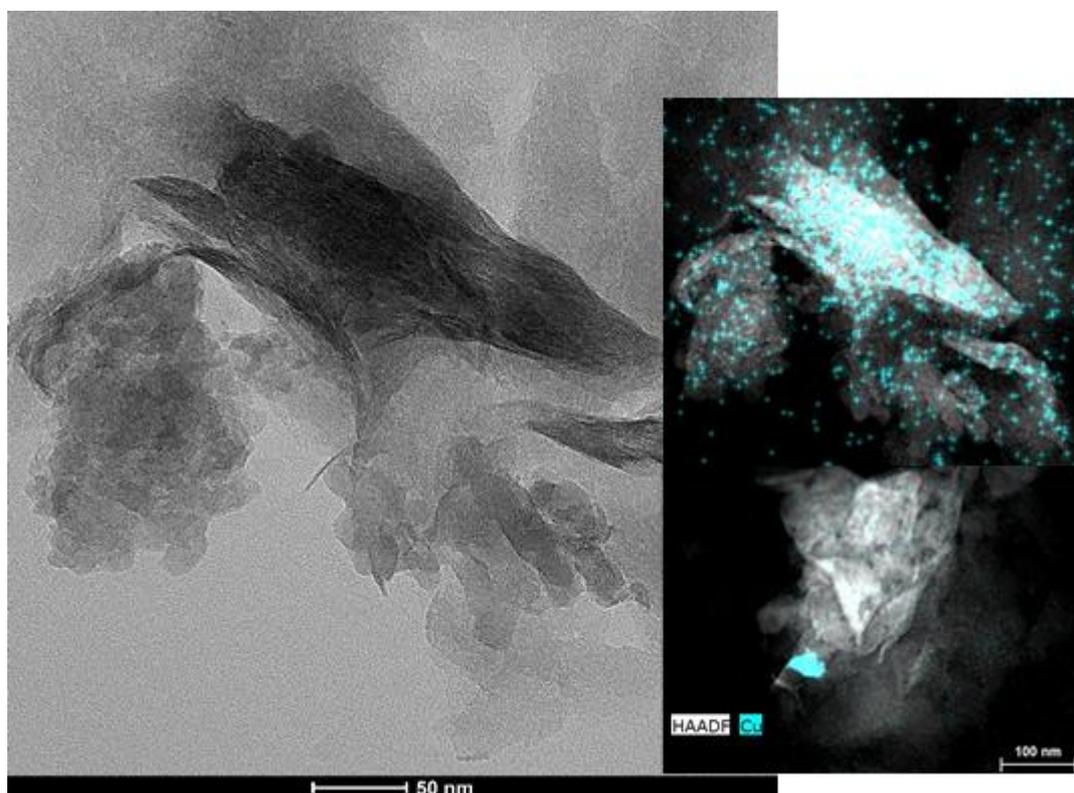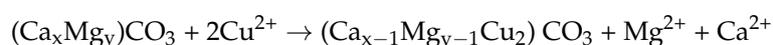
Figure 4. TEM micrograph of Cu-volcanic glass.

The adsorption isotherm of the raw volcanic glass reveals that Cu^{2+} species are adsorbed at low c_{eq} values (Figure 3). These data suggest a strong interaction between raw volcanic glass and the Cu^{2+} species, as was reported from the K_L values (Table 3). The acid activation of volcanic glass causes a decrease in the adsorption capacity, probably due to a slight dissolution of the carbonate species by the acid solution. In these cases, Cu^{2+} adsorption could be ascribed mainly to the interaction of the Cu^{2+} species with the silanol groups. The strength of this interaction is lower, as indicated by the isotherm profiles and the K_L values. However, K_L values for this material are in line with those found in the literature for other materials: 0.024 L/mg for chitosan-based materials [53]; 8–10 L/mg, depending on the temperature, for functional Poly-Ethylene Terephthalate (PET) fibers [54]; 0.002–0.0006 L/mg for carbon nanotube–mullite composites [55]; 0.015–0.239 L/mg for multiadsorbent systems containing tea waste and dolomite [56]; and 0.098–0.26 for nanocomposites of ZnO with montmorillonite [57].

To sum up, volcanic glass is an efficient material for the adsorption of heavy metals such as Cu. The presence of minor impurities of carbonate species improves Cu adsorption capacity by stronger chemical interactions. These Cu adsorption values are below those of other adsorbents, such as zeolites and activated carbons, due to these materials display high specific surface area and/or microporosity. Nonetheless, volcanic glass displays quite interesting Cu adsorption values, taking into account that this material is inexpensive and highly available.

5. Light N-Paraffin Separation in Volcanic Glass

Cuban volcanic glass and volcanic glass with higher Cu adsorption capacity, i.e., the sample without acid treatment activation, were chosen to evaluate their capacity to separate *n*-paraffins. The chromatographic profiles of the *n*-paraffin mixtures are compiled in Figure 5 for raw volcanic glass and Cu-volcanic glass. Taking into account the profiles of all experiments, it can be observed how each paraffin is eluted at a different retention time, so both samples are appropriate materials for the separation of n-paraffins. In all cases, the chromatographic peaks were sufficiently sharp and symmetric to consider the Henry zone, since the interactions with neighboring molecules must be nonspecific or show low intensity.
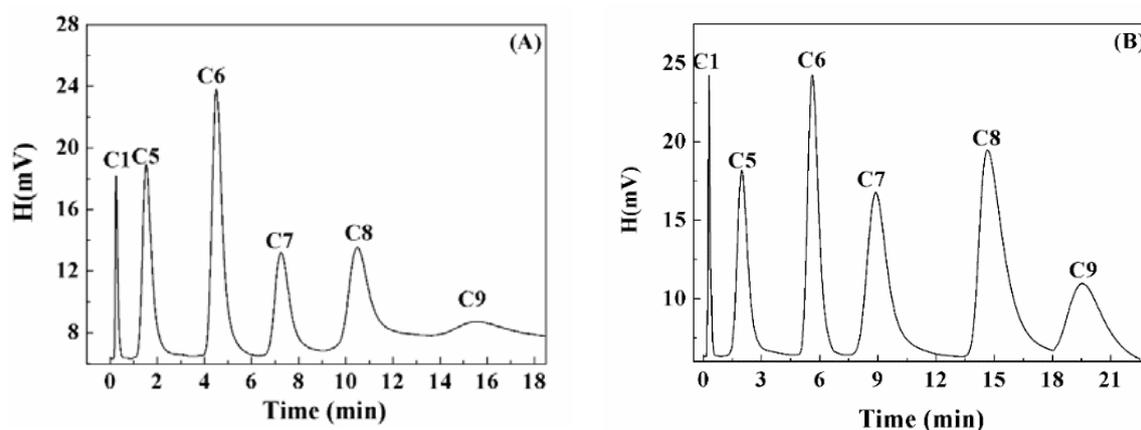
Figure 5. Chromatograms of CH_4 + C_5–C_9 mixture in (**A**) volcanic glass and (**B**) Cu^{2+}-volcanic glass. T_C = 400 K + 5 K/min.

As indicated, the adsorption of *n*-paraffins, which are only composed of C–C and C–H bonds, must be governed by nonspecific interactions. On the other hand, volcanic glass is an amorphous structure, mainly macroporous, although it also displays a certain microporosity (Figure 1). Thus, it is expected that the microporosity of volcanic glass can act as a molecular sieve for the separation of *n*-paraffins, as occurs with activated carbon and zeolites. In addition, it must be considered that the structure of volcanic glass expands with increased temperature, which could facilitate accessing n-paraffins inside the pores of volcanic glass. This can improve diffusion of the paraffins along the volcanic glass column, diminishing retention time.

The representation of (ln Vn) vs. (1/Tc) for each n-paraffin (Figure 6) can be fitted linearly, with R > 0.99 in all cases. The differential adsorption heat was determined from the slope, as shown in Table 3. These data reveal that adsorption heat is directly related to the length of the hydrocarbon, with the highest values obtained for nonane.

$$Q_d\ C_9H_{20} > Q_d\ C_8H_{18} > Q_d\ C_7H_{16} > Q_d\ C_6H_{14} > Q_d\ C_5H_{12}$$

Table 3 also reports how Cu-volcanic glass reaches higher adsorption heat values compared with raw volcanic glass. It is well known that transition metals, such as Ag, Cu, Co, and Ni, tend to interact with the double bond of the olefins [58]. The presence of these transition metals favors selective adsorption between olefins and saturated hydrocarbons with similar physicochemical properties, as takes place in propane-propylene separation. In the case of paraffins, the interactions between the Cu^{2+} species and C–H and C–H bonds should be negligible. Recently, Moreno-González et al. reported the existence of Cu^{2+}-alkane interactions by hyperfine sublevel correlation spectroscopy and electron paramagnetic resonance. Thus, it would be expected that the interaction between liquid *n*-paraffins and Cu^{2+} would lead to greater retention time and increased adsorption heat [59].
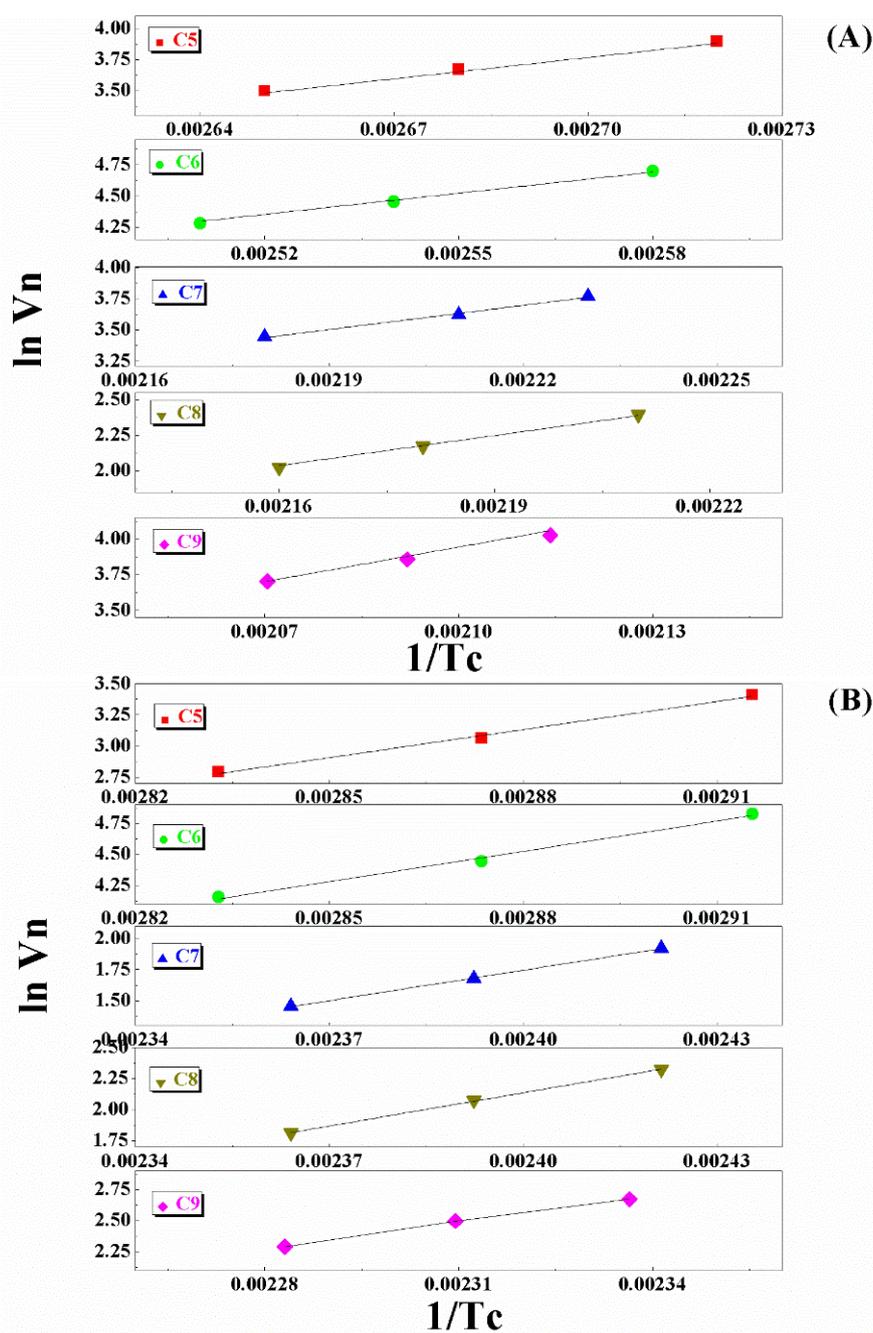
Figure 6. Ln Vn vs. 1/Tc representation by C_5–C_9 in (**A**) volcanic glass and (**B**) Cu^{2+}-volcanic glass.

The contribution of each $-CH_2-$ of the *n*-paraffins can be determined from the slope of the representation (adsorption heat vs. type of n-paraffin) (Figure 7), obtaining a Q_{dif} of 5.3 kJ/mol for raw volcanic glass, while Cu-volcanic glass only reaches a Q_{dif} of 4.2 kJ/mol (Table 4). In this way, previous research separated propane–propylene by inverse gas chromatography, indicating that propylene, which displays a stronger adsorbent–adsorbate interaction by the presence of the double bond, exhibits lower Q_{dif} in comparison to propane [20]. In this sense, the incorporation of Cu species into volcanic glass also causes a stronger interaction with n-paraffins, which could be related to a decrease of its Q_{dif} value. The variations of adsorption heat values between the n-paraffins are much higher than 1, confirming that both samples display an excellent capacity for separating *n*-paraffins.

Table 4. Fitting parameters of the adsorption isotherms of C_5–C_9 on volcanic glass and Cu^{2+}-volcanic glass at 273 K.

Sample	N-Paraffin	y = ax + b		r	Q_{dif}
		a	b		
	C5	5560	−11.23	0.995	46.2
	C6	6170	−11.23	0.997	51.3
Volcanic Glass	C7	6670	−11.11	0.995	55.4
	C8	7406	−13.97	0.993	61.5
	C9	8117	−13.10	0.995	67.4
	C5	6932	−16.83	0.991	57.6
	C6	7410	−16.81	0.990	61.6
Cu^{2+}-Volcanic Glass	C7	7810	−16.98	0.998	64.9
	C8	8669	−17.93	0.998	69.5
	C9	8969	−17.41	0.998	74.5
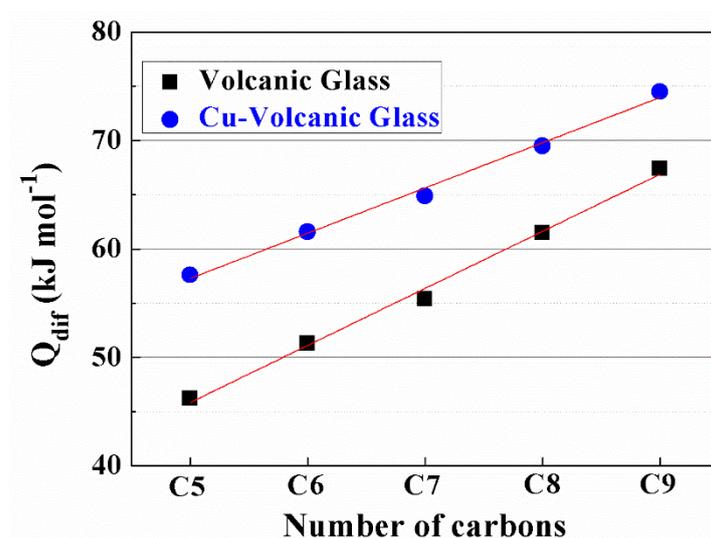
Figure 7. Representation of Q_{dif} vs. carbon number of the paraffin (C_5–C_9).

The adsorption heat of raw volcanic glass and Cu-volcanic glass was compared with other data reported in the literature using inverse gas chromatography under similar reaction conditions. Thus, the adsorption heat of both samples is in the same range as MOFs such as Cu–BTC [10] and natural zeolites such as clinoptilolite [7], so the use of inverse gas chromatography with inexpensive materials such as volcanic glass is a sustainable alternative to the traditional distillation to separate olefins/paraffins or several n-paraffins with different alkyl chains [20].

6. Conclusions

In the present paper, the use of natural volcanic glass from Cuba as an adsorbent in the removal of Cu^{2+} from dyes and its subsequent use to separate a mixture of *n*-paraffins by IGC were evaluated. It achieved great results in the copper removal experiments, related to the calcium carbonate content present. Copper replaces calcium from calcite during the adsorption process. Moreover, due to the partial solution of carbonates after acid activation, the sample without acid pretreatment achieved better copper removal results. Moreover, the Cu-containing sample was further studied in IGC to

separate olefins, and great separation results were achieved. The results were also compared with bare mineral. In both cases, separation of the mixture was achieved. Several factors play important roles in the separation process: microporosity, hydroxy groups, and copper species. Its high availability, low cost, capacity to operate at low temperatures, and stability make this material a potential and attractive candidate to be used in both heavy metal removal and paraffin separation for industrial purposes.

Author Contributions: M.A. and J.M.L.-S. designed the experiments and prepared the materials. J.A.C., A.I.-M., and E.R.-C. performed the experiments and characterizations and wrote the paper in collaboration with M.A.

Conflicts of Interest: The authors declare no conflict of interest.

References

1. Bryan, P.F. Removal of Propylene from Fuel-Grade Propane. *Sep. Purif. Rev.* **2004**, *33*, 157–182. [CrossRef]
2. Merkel, T.C.; Blanc, R.; Ciobanu, I.; Firat, B.; Suwarlim, A.; Zeid, J. Silver salt facilitated transport membranes for olefin/paraffin separations: Carrier instability and a novel regeneration method. *J. Membr. Sci.* **2013**, *447*, 177–189. [CrossRef]
3. Eldridge, R.B. Olefin/paraffin separation technology: A review. *Ind. Eng. Chem. Res.* **1993**, *32*, 2208–2212. [CrossRef]
4. Azhin, M.; Kaghazchi, T.; Rahmani, M. A review on olefin/paraffin separation using reversible chemical complexation technology. *J. Ind. Eng. Chem.* **2008**, *14*, 622–638. [CrossRef]
5. Faiz, R.; Li, K. Olefin/paraffin separation using membrane based facilitated transport/chemical absorption techniques. *Chem. Eng. Sci.* **2012**, *73*, 261–284. [CrossRef]
6. Ferreira, A.F.P.; Mittelmeijer-Hazeleger, M.C.; Granato, M.A.; Martins, V.F.D.; Rodrigues, A.E.; Rothenberg, G. Sieving di-branched from mono-branched and linear alkanes using ZIF-8: Experimental proof and theoretical explanation. *Phys. Chem. Chem. Phys.* **2013**, *15*, 8795–8804. [CrossRef] [PubMed]
7. Rivera, A.; Farías, T.; de Ménorval, L.C.; Autié-Castro, G.; Yee-Madeira, H.; Contreras, J.L.; Autié-Castro, M. Acid natural clinoptilolite: Structural properties against adsorption/separation of n-paraffins. *J. Colloid Interface Sci.* **2011**, *360*, 220–226. [CrossRef] [PubMed]
8. Huang, H.; He, Z.; Yuan, H.; Chen, Y.; Kobayashi, N. Evaluation of n-butane gas adsorption performance of composite adsorbents used for carbon canister. *Procedia Eng.* **2011**, *18*, 78–85. [CrossRef]
9. Yahia, S.B.; Ouederni, A. Hydrocarbons gas storage on activated carbons. *Int. J. Chem. Eng. Appl.* **2012**, *3*, 220–227. [CrossRef]
10. Herm, H.; Bloch, E.D.; Long, J.R. Hydrocarbon separation in metal-organic frameworks. *Chem. Mater.* **2014**, *26*, 323–338. [CrossRef]
11. Bhadra, B.N.; Jhung, S.H. Selective adsorption of *n*-alkanes from *n*-octane on metal-organic frameworks: Length selectivity. *ACS Appl. Mater. Interf.* **2016**, *8*, 6370–6777. [CrossRef]
12. Rivera, A.; Farías, T.; de Ménorval, L.C.; Ruiz-Salvador, A.R. Preliminary characterization of drug support systems based on natural clinoptilolite. *Microporous Mesoporous Mater.* **2003**, *61*, 249–259. [CrossRef]
13. Elizalde-González, M.P.; Pérez-Cruz, M.A. Interaction between organic vapors and clinoptilolite–mordenite rich tuffs in parent, decationized, and lead exchanged forms. *J. Colloid Interface Sci.* **2007**, *312*, 317–325. [CrossRef] [PubMed]
14. Hernández, M.A.; Corona, L.; González, A.I.; Rojas, F.; Lara, V.H.; Silva, F. Quantitative study of the adsorption of aromatic hydrocarbons (Benzene, Toluene, and *p*-Xylene) on dealuminated clinoptilolites. *Ind. Eng. Chem. Res.* **2005**, *44*, 2908–2916. [CrossRef]
15. Ruggieri, F.; Marín, V.; Gimeno, D.; Fernández-Turiel, J.L.; García-Vallés, M.; Gutiérrez, L. Application of zeolitic volcanic rocks for arsenic removal from water. *Eng. Geol.* **2008**, *101*, 245–250. [CrossRef]
16. Steinhauser, G.; Bichler, M. Adsorption of ions onto high silica volcanic glass. *Appl. Radiat. Isotopes* **2008**, *66*, 1–8. [CrossRef] [PubMed]
17. Dogan, M.; Alkan, M. Removal of methyl violet from aqueous solution by perlite. *J. Colloid Interface Sci.* **2003**, *267*, 32–41. [CrossRef]

18. Alkan, M.; Dogan, M. Adsorption kinetics of Victoria blue onto perlite. *Fresenius Environ. Bull.* **2003**, *12*, 418–425.

19. Dogan, M.; Alkan, M.; Turkylmaz, A.; Ozdemir, Y. Kinetics and mechanism of removal of methylene blue by adsorption onto perlite. *J. Hazard. Mater.* **2004**, *109*, 141–148. [PubMed]

20. Fernández-Hechevarría, H.M.; Labadie-Suárez, J.M.; Santamaría-González, J.; Infantes-Molina, A.; Autié-Castro, G.; Cavalcante, C.L., Jr.; Rodríguez-Castellón, E.; Autié-Castro, M. Adsorption and separation of propane and propylene by Cuban natural volcanic glass. *Mater. Chem. Phys.* **2015**, *168*, 132–137. [CrossRef]

21. Friedman, I.; Long, W. Volcanic glasses, their origins and alteration processes. *J. Non-Cryst. Solid* **1984**, *67*, 127–133. [CrossRef]

22. Buck, B.A. Ancient technology in contemporary surgery. *West. J. Med.* **1982**, *136*, 265–269. [PubMed]

23. Disa, J.J.; Vossoughi, J.; Goldberg, N.H. A comparison of obsidian and surgical steel scalpel wound healing in rats. *Plast. Reconstr. Surg.* **1993**, *92*, 884–887. [CrossRef] [PubMed]

24. Alkan, M.; Dogan, M. Adsorption of copper(II) onto perlite. *J. Colloid Interface Sci.* **2001**, *243*, 280–291. [CrossRef]

25. Tomita, K.; Yamane, H.; Kawano, M. Synthesis of smectite from volcanic glass at low temperature. *Clay Clay Miner.* **1993**, *41*, 655–661. [CrossRef]

26. Yoshida, A.; Inoue, K. Formation of faujasite-type zeolite from ground Shirasu volcanic glass. *Zeolites* **1986**, *6*, 467–473. [CrossRef]

27. Yoshida, A.; Inoue, K. Whiteness in zeolite A prepared from Shirasu volcanic glass. *Zeolites* **1988**, *8*, 94–100. [CrossRef]

28. Rivas, L.; Villegas, S.; Ruf, B.; Peric, I. Removal of metal ions with impact on the environment by wate-insolutble functional copolymer: Synthesis and metal ion uptake properties. *J. Chil. Chem. Soc.* **2007**, *52*, 1164–1168. [CrossRef]

29. Ground Water and Drinking Water. Available online: https://www.epa.gov/ground-water-and-drinking-water/national-primary-drinking-water-regulations (accessed on 16 February 2018).

30. Bereket, G.; Aroguz, A.Z.; Ozel, M.Z. Removal of Pb(II), Cd(II), Cu(II), and Zn(II) from aqueous solutions by adsorption on bentonite. *J. Colloid Interface Sci.* **1997**, *187*, 338–343. [CrossRef] [PubMed]

31. Autié-Castro, G.; Autié, M.; Reguera, E.; Santamaría-González, J.; Moreno-Tost, R.; Rodríguez-Castellón, E.; Jiménez-López, A. Adsorption and separation of light alkane hydrocarbons by porous hexacyanocobaltates (III). *Surf. Interf. Anal.* **2009**, *41*, 730–734. [CrossRef]

32. Voelkel, A.; Strzemiecka, B.; Adamska, K.; Milczewska, K. Inverse gas chromatography as a source of physiochemical data. *J. Chromatogr. A* **2009**, *1216*, 1551–1566. [CrossRef] [PubMed]

33. Mohammadi-Jan, S.; Waters, K.E. Inverse gas chromatography applications: A review. *Adv. Colloid Interface Sci.* **2014**, *212*, 21–44. [CrossRef] [PubMed]

34. Batko, K.; Voelkel, A. Inverse gas chromatography as a tool for investigation of nanomaterials. *J. Colloid Interface Sci.* **2007**, *315*, 768–771. [CrossRef] [PubMed]

35. Menzel, R.; Lee, A.; Bismarck, A.; Shaffer, M.S.P. Inverse gas chromatography of as-received and modified carbon nanotubes. *Langmuir* **2009**, *25*, 8340–8348. [CrossRef] [PubMed]

36. Heng, J.Y.Y.; Pears, D.F.; Thielmann, F.; Lampke, T.; Bismark, A. Methods to determine surface energies of natural fibres: A review. *Compos. Interface* **2007**, *14*, 581–604. [CrossRef]

37. Murakami, Y.; Enoki, R.; Ogoma, Y.; Kondo, Y. Studies on interaction between silica gel and polymer blend by inverse gas chromatography. *Polym. J.* **1998**, *30*, 520–525. [CrossRef]

38. Abel, M.L.; Chehimi, M.M.; Fricker, F.; Delamar, M.; Brown, A.M.; Watts, J.F. Adsorption of poly(methyl methacrylate) and poly(vinyl chloride) blends onto polypyrrole: Study by X-ray photoelectron spectroscopy, time-of-flight static secondary ion mass spectroscopy, and inverse gas chromatography. *J. Chromatogr. A* **2002**, *969*, 273–285. [CrossRef]

39. Brunauer, S.; Emmett, P.H.; Teller, E. Adsorption of gases in multimolecular layers. *J. Am. Chem. Soc.* **1938**, *60*, 309–319. [CrossRef]

40. Langmuir, I. The adsorption of gases on plane surfaces of glass, mica and platinum. *J. Am. Chem. Soc.* **1918**, *40*, 1361–1403. [CrossRef]

41. Thommes, M.; Kaneko, K.; Neimark, A.V.; Olivier, J.P.; Rodriguez-Reinoso, F.; Rouquerol, J.; Sing, K.S.W. Physisorption of gases, with special reference to the evaluation of surface area and pore size distribution (IUPAC Technical Report). *Pure Appl. Chem.* **2015**, *87*, 1051–1069. [CrossRef]

42. Madejová, J. FTIR techniques in clay mineral studies. *Vib. Spectrosc.* **2003**, *31*, 1–10. [CrossRef]

43. Farmer, V.C. (Ed.) *Infrared Spectra of Minerals*; Mineralogical Society: London, UK, 1974; p. 331.

44. Vilarrasa-García, E.; Cecilia, J.A.; Azevedo, D.C.S.; Cavalcante, C.L., Jr.; Rodríguez-Castellón, E. Evaluation of porous clay heterostructures modified with amine species as adsorbent for the CO_2 capture. *Microporous Mesoporous Mater.* **2017**, *249*, 25–33. [CrossRef]

45. Correia, L.M.; Campelo, N.S.; Novaes, D.S.; Cavalcante, C.L., Jr.; Cecilia, J.A.; Rodríguez-Castellón, E.; Vieira, R.S. Characterization and application of dolomite as catalytic precursor for canola and sunflower oils for biodiesel production. *Chem. Eng. J.* **2015**, *269*, 35–43. [CrossRef]

46. Moulder, J.F.; Stickle, W.F.; Sool, P.E.; Bomber, K.D. *Handbook of X-Ray Photoelectron Spectroscopy*; Pekin-Elmer: Eden Praire, NM, USA, 1992.

47. Kinniburgh, D.G. *Adsorption of Inorganic Solid–Liquid Interfaces*; Anderson, M.A., Rubin, A.J., Eds.; Ann Arbor Science Publisher: Ann Arbor, MI, USA, 1981; pp. 91–160.

48. Ghassabzadeh, H.; Torab-Mostaedi, M.; Mohaddespour, A.; Maragheh, M.G.; Ahmadi, S.J.; Zaheri, P. Characterizations of Co(II) and Pb(II) removal process from aqueous solutions using expanded perlite. *Desalinitation* **2010**, *261*, 73–79. [CrossRef]

49. Ghassabzadeh, H.; Mohadespour, A.; Torab-Mostaedic, M.; Zaherib, P.; Maraghehc, M.G.; Taheric, H. Adsorption of Ag, Cu and Hg from aqueous solutions using expanded perlite. *J. Hazard. Mater.* **2010**, *177*, 950–955. [CrossRef] [PubMed]

50. Franco, F.; Pozo, M.; Cecilia, J.A.; Benítez-Guerrero, M.; Pozo, E.; Martín Rubí, J.A. Microwave assisted acid treatment of sepiolite: The role of composition and "crystallinity". *Appl. Clay Sci.* **2014**, *102*, 15–27. [CrossRef]

51. Franco, F.; Pozo, M.; Cecilia, J.A.; Benítez-Guerrero, M.; Lorente, M. Effectiveness of microwave assisted acid treatment on dioctahedral and trioctahedral smectites. The influence of octahedral composition. *Appl. Clay Sci.* **2016**, *120*, 70–80. [CrossRef]

52. Cecilia, J.A.; Arango-Díaz, A.; Rico-Pérez, V.; Bueno-López, A.; Rodríguez-Castellón, E. The influence of promoters (Zr, La, Tb, Pr) on the catalytic performance of CuO-CeO_2 systems for the preferential oxidation of CO in the presence of CO_2 and H_2O. *Catal. Today* **2015**, *253*, 115–125. [CrossRef]

53. Niua, Y.; Li, K.; Ying, D.; Wang, J.; Jia, J. Novel recyclable adsorbent for the removal of copper(II) and lead(II) from aqueous solution. *Bioresour. Technol.* **2017**, *229*, 63–68. [CrossRef] [PubMed]

54. Niu, Y.; Ying, D.; Li, K.; Wang, Y.; Jia, J. Fast removal of copper ions from aqueous solution using an eco–friendly fibrous adsorbent. *Chemosphere* **2016**, *161*, 501–509. [CrossRef] [PubMed]

55. Tofighy, M.A.; Mohammadi, T. Copper ions removal from water using functionalized carbon nanotubes–mullite composite as adsorbent. *Mater. Res. Bull.* **2015**, *68*, 54–59. [CrossRef]

56. Albadarin, A.B.; Mo, J.; Glocheux, Y.; Allen, S.; Walker, G.; Mangwandi, C. Preliminary investigation of mixed adsorbents for the removal of copper and methylene blue from aqueous solutions. *Chem. Eng. J.* **2014**, *255*, 525–534. [CrossRef]

57. Abubakar, H.; Ahmad, M.; Hussein, M.Z.; Ibrahim, N.A.; Musa, A.; Saleh, T.A. Nanocomposite of ZnO with montmorillonite for removal of lead and copper ions from aqueous solutions. *Process Saf. Environ. Prot.* **2017**, *109*, 97–105.

58. Grande, C.A.; Araujo, J.D.P.; Cavenati, S.; Firpo, N.; Basaldella, E.; Rodrigues, A.E. New π-complexation adsorbents for propane-propylene separation. *Langmuir* **2004**, *20*, 5291–5297. [CrossRef] [PubMed]

59. Moreno-González, M.; Palomares, A.E.; Chiesa, M.; Boronat, M.; Giamello, E.; Blasco, T. Evidence of a Cu^{2+}–alkane interaction in Cu-zeolite catalysts crucial for the selective catalytic reduction of NO_x with hydrocarbons. *ACS Catal.* **2017**, *7*, 3501–3509. [CrossRef]